1-1-2011

Actin depolymerizing factor controls actin turnover and gliding motility in Toxoplasma gondii

Simren Mehta
Washington University School of Medicine in St. Louis

L. David Sibley
Washington University School of Medicine in St. Louis

Actin depolymerizing factor controls actin turnover and gliding motility in *Toxoplasma gondii*

Simren Mehta and L. David Sibley
Department of Molecular Microbiology, Washington University School of Medicine, St. Louis, MO 63110

ABSTRACT **Apicomplexan parasites rely on actin-based gliding motility to move across the substratum, cross biological barriers, and invade their host cells. Gliding motility depends on polymerization of parasite actin filaments, yet ~98% of actin is nonfilamentous in resting parasites. Previous studies suggest that the lack of actin filaments in the parasite is due to inherent instability, leaving uncertain the role of actin-binding proteins in controlling dynamics. We have previously shown that the single allele of *Toxoplasma gondii* actin depolymerizing factor (TgADF) has strong actin monomer–sequestering and weak filament-severing activities in vitro. Here we used a conditional knockout strategy to investigate the role of TgADF in vivo. Suppression of TgADF led to accumulation of actin-rich filaments that were detected by immunofluorescence and electron microscopy. Parasites deficient in TgADF showed reduced speed of motility, increased aberrant patterns of motion, and inhibition of sustained helical gliding. Lack of TgADF also led to severe defects in entry and egress from host cells, thus blocking infection in vitro. These studies establish that the absence of stable actin structures in the parasite are not simply the result of intrinsic instability, but that TgADF is required for the rapid turnover of parasite actin filaments, gliding motility, and cell invasion.**

Monitoring Editor
Yu-Li Wang
Carnegie Mellon University

Received: Dec 3, 2010
Revised: Jan 31, 2011
Accepted: Feb 11, 2011

INTRODUCTION

Apicomplexan parasites require filamentous actin for the unique process of gliding motility, a substrate-dependent form of movement that differs from amoeboid movements of crawling cells and does not rely on cilia or flagella (Sibley, 2004). Instead, the parasite undergoes counterclockwise circular patterns that follow the curvature of the crescent-shaped cell or clockwise helical rotations along the long axis, as it migrates across the substratum (Håkansson *et al.*, 1999). Gliding is mediated by translocation of transmembrane surface adhesins along the parasite surface via connection to the actomyosin cytoskeleton that is transiently assembled underneath the parasite plasma membrane (Sibley, 2004). Repeated cycles of host cell invasion, replication, and egress are required for parasite survival, and both entry and exit from host cells require polymerization of actin in the parasite.

Cytochalasin D blocks parasite gliding, cell invasion, and egress, and genetic studies have shown that this blocking is caused by an absolute requirement for filamentous actin in the parasite (Dobrowolski and Sibley, 1996). Despite the importance of actin filaments, >98% of actin is unpolymerized in *Toxoplasma gondii* and in *Plasmodium* spp. (Dobrowolski *et al.*, 1997; Pinder *et al.*, 1998). For example, actin filaments are undetectable in parasites by sedimentation, phalloidin staining, or conventional microscopy techniques (Dobrowolski *et al.*, 1997; Shaw and Tilney, 1999), and filaments have been detected only transiently in membrane footprints of gliding *T. gondii* obtained by freeze-fracture electron microscopy (EM; Sahoo *et al.*, 2006). Overstimulation of actin polymerization by treatment with jasplakinolide (JAS) results in an abundance of filaments in *T. gondii*, yet treatment disrupts the normal process of gliding, resulting in uncoordinated movements and inhibition of host cell invasion (Poupel and Tardieux, 1999; Wetzel *et al.*, 2004). Collectively, these studies predict that parasite actin filaments are rapidly assembled and disassembled during gliding, although the regulatory mechanisms that normally control actin dynamics in vivo remain largely unknown.

This article was published online ahead of print in MBoC in Press (http://www.molbiolcell.org/cgi/doi/10.1091/mbc.E10-12-0939) on February 23, 2011.

Address correspondence to: L. David Sibley (sibley@wustl.edu).

Abbreviations used: ACT, Actin; ADF, actin depolymerizing factor; Atc, anhydrous tetracycline; cKO, conditional knockout; EM, electron microscopy; HFF, human foreskin fibroblast; JAS, jasplakinolide; PRF, profilin; Tet-TA, tetracycline transactivator; TgADF, *Toxoplasma gondii* ADF.

T. gondii expresses one actin allele, TgACT1, that has 83% identity to vertebrate actin and is expressed throughout the parasite life cycle (Dobrowolski *et al.*, 1997). Parasite actin filaments are inherently less stable than the conventionally studied actins from yeast or vertebrate cells (Schmitz *et al.*, 2005; Sahoo *et al.*, 2006), a property that may arise from key molecular substitutions at the monomer–monomer interface along the filament (Sahoo *et al.*, 2006). The absence of stable actin filaments has led to a model suggesting that the absence of F-actin in the parasite is largely attributable to intrinsic instability of the polymer. The limited repertoire of actin binding proteins found in apicomplexan parasites also suggests that actin dynamics may be intrinsically governed. Although apicomplexan parasites do contain homologues for formins, profilin (PRF), actin depolymerizing factor (ADF)/cofilin, capping protein, cyclase-associated protein, and coronin (Baum *et al.*, 2006; Schüler and Matuschewski, 2006), the mechanisms by which these proteins influence actin dynamics in vivo is largely unknown.

ADF/cofilin proteins are essential for controlling cell polarity, migration, and division in a variety of systems from yeast, amoeba, worms, and vertebrates (Bamburg, 1999; Ono, 2007). ADF/cofilin proteins are thought to increase filament turnover by binding to the sides of actin filaments and changing the twist of the filament, leading to severing of the filament (McGough *et al.*, 1997) and/or increased turnover of subunits (Carlier *et al.*, 1997). More recently, a subset of ADF/cofilin proteins have been shown to have potent monomer sequestering activity, which may also influence actin dynamics (Yamashiro *et al.*, 2005). Most apicomplexans express a single ADF isoform (Baum *et al.*, 2006), with the exception of Plasmodium, which has two isoforms referred to as PfADF1 and PfADF2 (Schachtele *et al.*, 1988; Schuler *et al.*, 2005; Doi *et al.*, 2010). Using in vitro biochemical assays with recombinant *T. gondii* ADF (TgADF), we have previously shown that this protein has strong actin monomer–sequestering properties and relatively weaker filament-severing activity compared with the prototypical yeast cofilin (Mehta and Sibley, 2010).

To investigate the role of ADF in regulating actin dynamics in vivo, we generated a conditional knockout (cKO) line for TgADF and examined the effect of suppression on the intracellular life cycle of *T. gondii*.

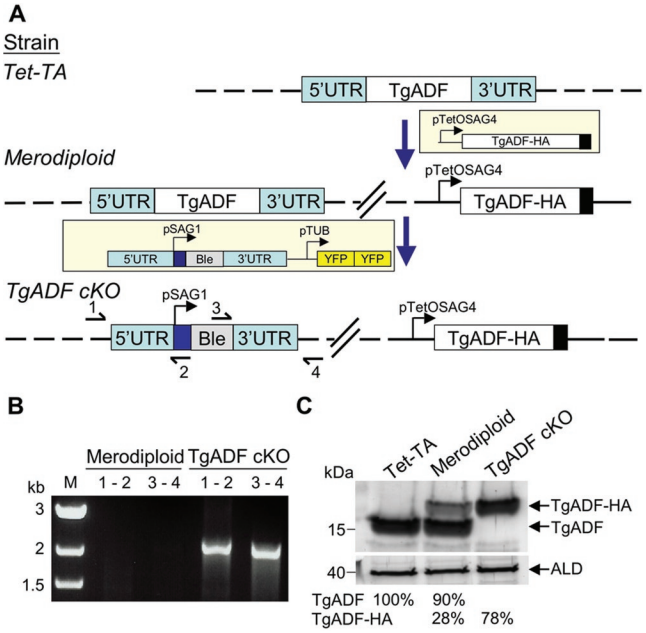

FIGURE 1: Generation of a cKO of TgADF. (A) Diagram outlining the strategy that was used to generate the cKO of *TgADF*. The Tet-TA strain was transfected with a plasmid containing HA-tagged *TgADF* (TgADF-HA) under the control of the Tet-regulatable promoter pTetOSag4 to generate the merodiploid strain. The endogenous *TgADF* gene was then replaced by the phleomycin resistance marker (*ble*) flanked by 5′ and 3′ untranslated regions (UTR). Double crossover events were screened for using tandem YFP (YFPYFP) as a negative selection marker. Diagnostic PCR primers 1–4 used to confirm the correct integration of the resistance marker are shown in the bottom panel. Dashed lines represent the chromosome of each strain. (B) PCR analysis demonstrating disruption of the *TgADF* locus. Diagnostic PCR primer pairs 1–2 and 3–4 depicted in (A) confirmed the successful replacement of the endogenous *TgADF* gene with the *ble* resistance cassette. Genomic DNA from the merodiploid strain was used as a negative control. M, marker lane. (C) Western blot analysis of TgADF expression. Aldolase (ALD) was used as a loading control. Phosphorimager quantitation of bands as a percentage of the endogenous TgADF protein in the Tet-TA strain.

RESULTS

Generation of a cKO of TgADF

In most systems studied to date, ADF is essential and null mutants are not viable (Bamburg, 1999). Therefore, we assessed the function of TgADF using the previously described tetracycline transactivator (Tet-TA) cKO system (Meissner *et al.*, 2002). *TgADF* was cloned with a C-terminal epitope tag under the control of the *SAG4* tetracycline-regulatable promoter and introduced into a strain of *T. gondii* that harbors a Tet-TA (Meissner *et al.*, 2002), to generate a merodiploid line (Figure 1A). To create the TgADF cKO, the endogenous *TgADF* gene was replaced by the *ble* selectable marker (Messina *et al.*, 1995) (Figure 1A). Correct integration of the *ble* gene at the endogenous *TgADF* locus was confirmed by PCR (Figure 1B). The deletion of the endogenous gene was confirmed at the protein level by Western blot analysis with rabbit anti-TgADF antibodies (Figure 1C). Consistent with the loss of the endogenous gene, only the tagged TgADF protein was detected in the cKO, where it was expressed at 78% of the endogenous level (Figure 1C).

Suppression of TgADF protein expression

To determine the degree of TgADF suppression, parasites were grown in the presence of anhydrous tetracycline (Atc, a noncytotoxic derivative of tetracycline) and examined by immunofluorescence microscopy. In untreated parasites, TgADF was dispersed evenly throughout the parasite cytosol (Figure 2A). After growth in Atc for 48 h, TgADF expression was suppressed to almost undetectable levels in the cKO (Figure 2A). As expected, the merodiploid strain, which also encodes the endogenous *TgADF* gene in addition to the regulatable allele, still expressed TgADF following treatment with Atc (Figure 2A). To examine the kinetics of shutdown, Western blot analysis was used to estimate TgADF protein levels in parasite lysates after treatment with Atc for varying time intervals (Figure 2B). Probing TgADF cKO parasites with anti-TgADF antibodies revealed ~20% expression after 24 h, dropping to 3% of initial levels after 48 h of Atc treatment (Figure 2B).

ADF cKO is severely compromised in host cell invasion and egress

We examined the effect of the absence of ADF on the *T. gondii* intracellular life cycle using a plaquing assay, which captures many aspects of intracellular growth, including invasion, replication, egress, and dissemination. The Tet-TA and merodiploid strains formed approximately the same number of plaques in the absence

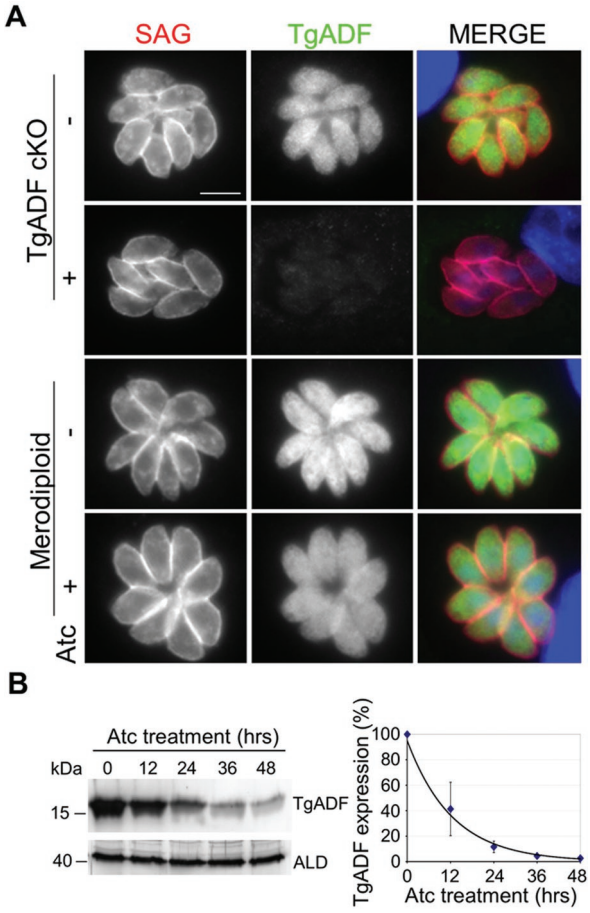

FIGURE 2: Suppression of TgADF protein expression. (A) Immunofluorescence analysis of TgADF repression in parasites cultured ± Atc for 48 h. TgADF (green) and SAG (red) were detected using rabbit anti-TgADF and mouse anti-SAG antibodies, respectively. Scale bar: 5 μm. (B) Western blot analysis of the time course of TgADF repression following Atc treatment. TgADF cKO parasites were treated with Atc for 0–48 h, and parasite lysates were probed with antibodies to TgADF or aldolase (ALD) as a loading control. Expression was quantified using phosphorimager analysis as a percentage compared with no treatment. Values represent means ± SEM (n = 3 experiments).

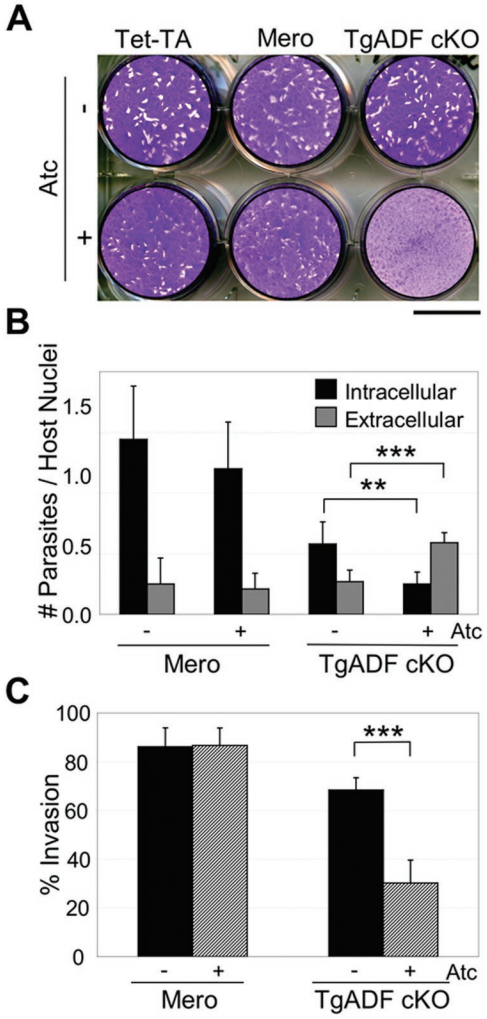

FIGURE 3: Effects of TgADF suppression on invasion. (A) Plaque assay of parasites grown ± Atc for 8 d on fibroblast monolayers. Scale bar: 2 cm. Plaques are distinguished as oval white spots on the purple background, representing areas where host cells have been destroyed by lytic growth. The lighter staining in the bottom right panel is characteristic of a situation where no parasite growth is detected and the monolayer remains intact. (B) Parasite invasion of host cell monolayers as detected by the two-color immunofluorescence assay. Parasites were treated ± Atc for 66 h, harvested, and allowed to invade host cells for 20 min before being fixed and differentially stained for the parasite surface antigen 1 (SAG1) to identify intracellular vs. extracellular parasites. Data are represented as the number of parasites invaded (intracellular) or attached (extracellular) per host cell nucleus. Values represent means ± SD, 3 samples from each of 2 experiments (n = 6). **$p \leq 0.005$, ***$p \leq 0.0001$. (C) The data from (B) are represented as the percentage of parasites that had invaded host cells.

or presence of Atc, although plaques were slightly smaller due to prolonged growth in Atc (Figure 3A). Although the TgADF cKO grew normally in the absence of Atc, no plaques were detected when TgADF cKO parasites were grown in the presence of Atc (Figure 3A). No inhibition of intracellular replication was observed over the first 36 h of culture in Atc (unpublished data), suggesting that this defect was not simply due to a block in growth of the parasite.

To examine the ability of the TgADF cKO to invade host cells, we used an assay to differentially detect intracellular from extracellular parasites, as described previously (Buguliskis *et al.*, 2010). Invasion by the merodiploid was similar in the presence and absence of Atc (Figure 3C). The TgADF cKO showed a slight reduction in invasion when grown in the absence of Atc, indicating that expression of the tagged allele is not fully wild type, even though it is sufficient to support growth (Figure 3C). Regardless of this modest defect, treatment of the TgADF cKO with Atc led to a significant further decrease in the number of intracellular parasites, with a corresponding increase in extracellular parasites (Figure 3C). Similarly, when parasite invasion was examined as the percentage of parasites that had invaded, suppression of TgADF resulted in a significant decrease in invasion over the untreated TgADF cKO (Figure 3C).

To determine whether TgADF suppression affected egress by *T. gondii*, we used time-lapse video microscopy to examine parasite exit from mature vacuoles stimulated with calcium ionophore A23187, as described previously (Endo *et al.*, 1982). Parasites were monitored to determine the onset of motility, length of time for egress, and dissemination from the infected host cell. The merodiploid and untreated TgADF cKO strains behaved similarly, initiating motility within the vacuole at ~1.5 min after ionophore stimulation

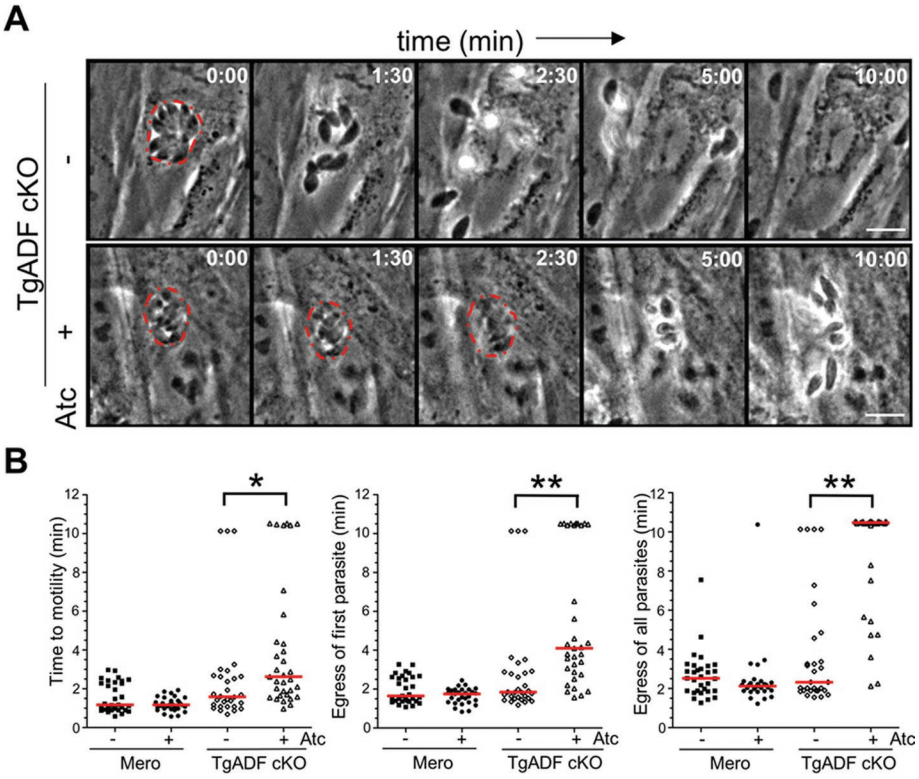

FIGURE 4: Effects of TgADF suppression on egress from host cells. (A) Time-lapse video micrographs comparing ionophore-induced egress of TgADF cKO parasites grown ± Atc for 66 h. Infected host cells were stimulated with 2 μM calcium ionophore A23187, and parasite egress from the parasitophorous vacuole was monitored over time. Vacuoles are outlined in red, and the time elapsed after ionophore addition is indicated in minutes:seconds. Scale bar: 10 μm. (B) Quantitation of the kinetics of egress based on time-lapse video microscopy. Times were plotted for the activation of parasite motility within the vacuole (left), egress of the first parasite from the vacuole (middle), and egress of all parasites from the vacuole (right) after the addition of ionophore. Parasites that did not leave the vacuole were assigned the value of the last time-point (10.5 min). At least 29 vacuoles were counted from two independent experiments. Bars represent the median time taken. Mann–Whitney U test, *p ≤ 0.005, **p ≤ 0.0001.

(Figure 4, A and B), and completing egress within the next 1.2 min (Table 1 and Supplementary Movie 1). In contrast, TgADF cKO parasites treated with Atc were slower to initiate motility (mean time 2.7 ± 1.1 min [± SD]) and displayed temporal heterogeneity in the time required to first become motile (Figure 4, A and B, and Supplemental Movie 2). Furthermore, even after motility was initiated, Atc-treated TgADF cKO parasites were slow to leave the vacuole, with one or more parasites still remaining inside the majority of vacuoles (24/33) after 10 min (Figure 4B and Table 1). After emerging from the vacuole, merodiploid and untreated TgADF cKO parasites were highly motile, often moving quite far from the original vacuole (Figure 4A and Supplemental Movie 1). In contrast, parasites in which TgADF had been suppressed were relatively nonmotile and remained close to the point of exit from the vacuole (Figure 4A and Supplemental Movie 2).

Effects of TgADF suppression on *T. gondii* gliding motility

To directly investigate the effect of TgADF suppression on motility, we used time-lapse video microscopy to examine extracellular parasites gliding on glass coverslips. Parasites expressing TgADF underwent multiple rounds of helical movement during the observation period (Figure 5B and Supplemental Movie 3). In contrast, suppression of TgADF by growth of the cKO in Atc led to a dramatic reduction in helical and circular gliding, compared with either the merodiploid or cKO cells grown in the absence of Atc (Figure 5A). In addition to the dramatic reduction in the frequency of several standard motility behaviors, suppression of TgADF led to extremely slow movement of parasites. For example, in the absence of TgADF, parasites were unable to complete even a single helical turn within the given time period, and instead underwent a slow serpentine movement that resulted in an elongated trail (Figure 5B and Supplemental Movie 4). These patterns were classified as short movements in the graphical representation in Figure 5A. Quantification of the speed of parasite movement revealed a slight reduction in the speed of both helical and circular gliding between the merodiploid strains and the TgADF cKO strain grown in the absence of Atc (Figure 5C and Table 2), consistent with the partial defect seen earlier in invasion assays. Nonetheless, suppression of TgADF resulted in a dramatic reduction in speed such that complete cycles of helical and circular movement were not typically observed in the course of the experiment (Figure 5C and Table 2). Additionally, there was an increased frequency of uncoordinated behaviors with the suppression of TgADF (Figure 5A). Such behaviors were characterized by frequent reversals of direction leading to no net movement, and were observed as back-and-forth rocking motions (see Supplemental Movie 5) or uncoordinated movements including "rolling" (see Supplemental Movie 6).

TgADF suppression leads to more stable actin in *T. gondii*

To examine if actin was more stable in the absence of TgADF, actin sedimentation assays were used to compare the ratio of

	Atc treatment	Average time to egress (min)[a]	Number of vacuoles with incomplete egress[b]
Merodiploid	–	1.1 ± 0.4[c]	1/30
Merodiploid	+	1.2 ± 0.7	0/29
TgADF cKO	–	1.2 ± 0.3	4/30[d]
TgADF cKO	+	4.2 ± 0.6*	24/33[e]

[a] Represents the average time taken from the initiation of motility to egress of the last parasite from the vacuole.
[b] Represents the number of vacuoles of the total number of vacuoles analyzed in which all of the parasites did not egress in 10 min.
[c] Mean time ± SD
[d] In 3 vacuoles, 0 parasites left the vacuole.
[e] In 8 vacuoles, 0 parasites left the vacuole.
* p ≤ 0.001 Student's *t* test, TgADF cKO – Atc versus TgADF cKO + Atc.

TABLE 1: Characterization of ionophore-induced egress in *T. gondii*.

unpolymerized and polymerized actin in parasite lysates (Figure 6A). Because parasite actin filaments are inherently less stable and do not form long actin filaments like conventional actins, parasite lysates were centrifuged at higher speeds, as has been previously reported (Mehta and Sibley, 2010). In parasites expressing TgADF, ~15% of parasite actin sedimented when centrifuged at 350,000 × *g* for 1 h (Figure 6A). In contrast, when TgADF was suppressed, the proportion of pelletable actin was significantly increased, indicating that in the absence of TgADF more parasite actin was found in the polymerized form (Figure 6A). To determine whether actin filaments could be visualized in these parasites, immunofluorescence microscopy was used to localize actin in extracellular parasites undergoing gliding. Previous work has shown that actin typically localizes diffusely in the cytoplasm with a perinuclear concentration in *T. gondii* (Dobrowolski *et al.*, 1997). In TgADF cKO parasites expressing ADF, actin was found predominantly in the cytoplasm with a perinuclear concentration (Figure 6B, –Atc). Following ADF suppression, the overall intensity of actin staining was not different, but actin was localized in a different pattern (Figure 6B, +Atc). Instead of the prominent central cytoplasmic staining, actin was concentrated at the periphery, especially at one or both poles of the parasite (Figure 6B, +Atc). In addition, short, cable-like structures were observed concentrated at the poles of the parasite (Figure 6B, middle), and these extended throughout the parasite cytoplasm tracing a spiral-like pattern (Figure 6B, right). Actin cables were detected in multiple planes of the parasite, as depicted in the z-series in Figure 6C, occurring both beneath the parasite membrane (Figure 6C, right) and internally in the cytosol (Figure 6C, left).

We used transmission EM to examine the ultrastructure of parasites and determine the nature of the actin-rich cables that occurred following suppression of TgADF. Consistent with previous reports (Wetzel *et al.*, 2003; Sahoo *et al.*, 2006), filamentous actin was not detected in parasites expressing ADF (Figure 7, A and D). Strikingly, following ADF suppression, actin filaments were detected underlying the parasite's inner membrane complex (Figure 7, B and C, arrowheads), often resulting in an apical protrusion rich with actin filaments (Figure 7B, arrow). Similar actin filament–rich structures were also observed at the basal end of parasites when ADF was suppressed (Figure 7, E and F). In cases where a basal protrusion was observed, it was accompanied by a break in the inner membrane (Figure 7E). In parallel, samples were prepared for cryoimmuno-EM, and actin was localized using a polyclonal rabbit anti-TgACT1 antibody as described previously (Dobrowolski *et al.*, 1997). Although the structure of the filaments was not preserved in cryoimmuno-EM, the anterior and posterior protrusions stained strongly with this specific antisera, demonstrating that these regions are rich in actin (Figure 7, G–I). Collectively, these data strongly suggest that stable actin filaments are formed in *T. gondii* in the absence of ADF.

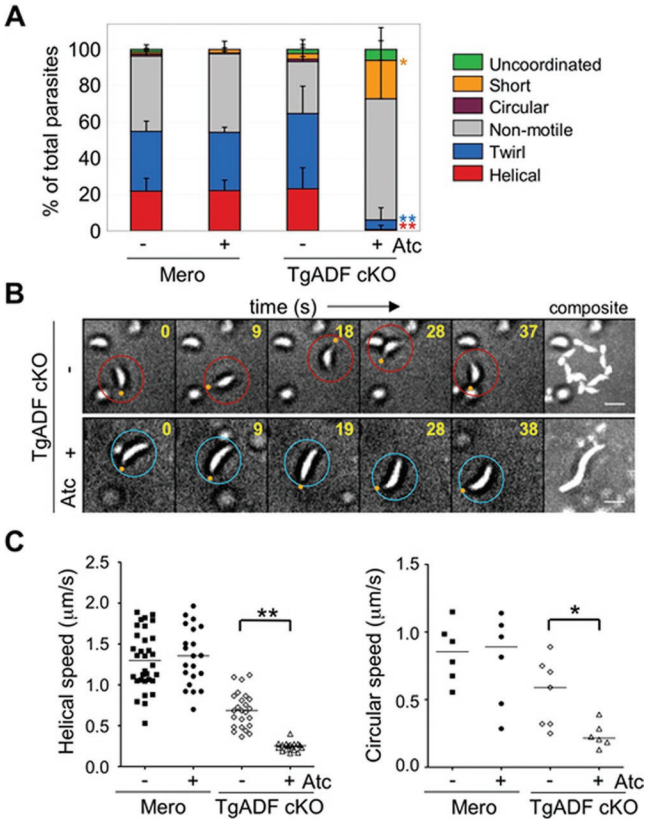

FIGURE 5: Effects of TgADF suppression on gliding motility. (A) Quantitation of parasite motility as observed by time-lapse video microscopy. Parasites were treated ± Atc for 66 h, harvested, and allowed to glide on BSA-coated, glass-bottom culture dishes. Motility was documented by time-lapse video microscopy. The type of motility was categorized as defined in *Materials and Methods*, and the data were plotted as a percentage of the total. Values represent means ± SD (n = 3 samples), from a representative of two similar experiments. Student's *t* test comparing TgADF cKO – Atc vs. TgADF cKO + Atc, *p ≤ 0.05, **p ≤ 0.01. (B) Time-lapse video micrographs comparing helical gliding in TgADF cKO parasites grown as in (A). Parasites of interest are highlighted with a circle (red, top panel; blue bottom panel), with the orange dot denoting the apical end. The last micrograph in both panels represents a summation of 45 s. Time elapsed shown in seconds in the top right-hand corner. Scale bar: 5 μm. (C) Scatter plots depicting speeds of helical (left), and circular (right), gliding motility in parasites treated as described in (A). The distance migrated by parasites was tracked over time based on time-lapse movies. Helical gliding speeds were calculated from following the movements of at least 15 parasites for each strain; circular speeds were based on following at least six parasites per strain. Bars represent median values. Mann–Whitney U test, *p ≤ 0.05; **p ≤ 0.001.

DISCUSSION

Apicomplexan parasites maintain their actin in a largely unpolymerized state, yet actin filaments are essential for gliding motility and host cell invasion. Here we investigated the function of TgADF in vivo using a cKO strategy. Suppression of ADF led to reduction in the speed of movement, formation of incomplete helical and circular turns, and more frequent direction reversals. Importantly these defects were associated with increased stability of parasite actin filaments, thus altering the normal balance of predominantly G-actin in the parasite. These findings demonstrate that dynamic turnover of actin in apicomplexan parasites is not simply due to intrinsic differences in polymer stability, but that TgADF plays a crucial role in regulating actin filament turnover in *T. gondii*.

Our results with suppression of TgADF are similar to those described in a previous report where suppression of *T. gondii* PRF disrupts motility and dramatically reduces egress (Plattner *et al.*, 2008). The greater magnitude of the PRF cKO in blocking egress likely reflects the different ways in which ADF and PRF regulate actin dynamics. Although PRF also likely sequesters actin monomers similar to TgADF, during gliding PRF is thought to act in concert with formin to promote filament polymerization and elongation (Baum *et al.*, 2008; Daher *et al.*, 2010). Although some ADF/cofilin proteins have been shown to induce actin polymerization (Bernstein and Bamburg, 2010), this is not the case for TgADF, which serves to sequester monomers and sever filaments (Mehta and Sibley, 2010).

Strain	Atc treatment	Type of motility			
				Short	
		Helical (μm/s)	Circular (μm/s)	Half-helix (μm/s)	Half-circle (μm/s)
Merodiploid	—	1.33 ± 0.13[a]	0.85 ± 0.09	—[b]	—
Merodiploid	+	1.38 ± 0.22	0.79 ± 0.14	—	—
TgADF cKO	—	0.69 ± 0.05*	0.48 ± 0.14	—	—
TgADF cKO	+	—	—	0.25 ± 0.01**	0.25 ± 0.01

[a] Mean speed ± SEM
[b] Behavior not observed.
* $p \leq 0.05$, Student's *t* test ADF cKO – Atc versus Merodiploid + Atc.
** $p \leq 0.005$, Student's *t* test TgADF cKO – Atc versus TgADF cKO + Atc.

TABLE 2: Comparison of rates of *T. gondii* gliding motility.

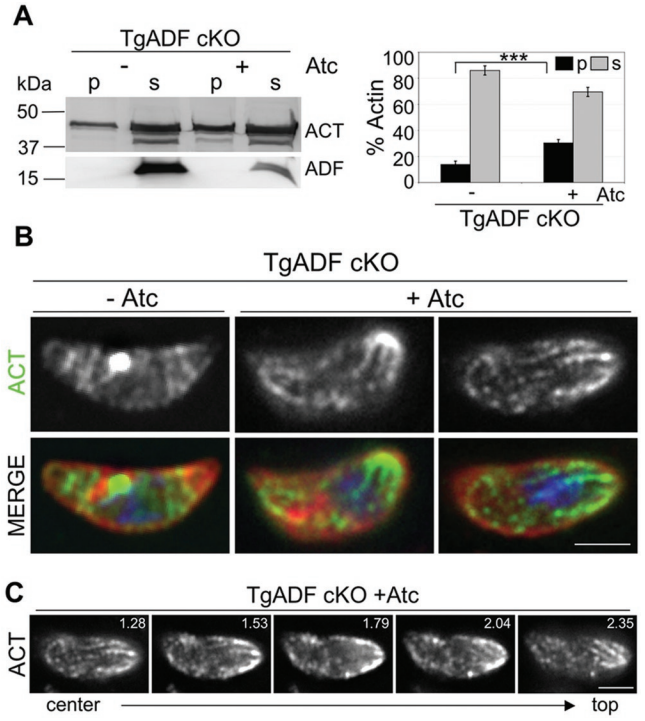

FIGURE 6: Effects of TgADF suppression on actin filament polymerization in *T. gondii*. (A) Sedimentation analysis of F-actin in TgADF cKO parasites grown ± Atc for 66 h. Parasite lysates were centrifuged at 350,000 × *g* for 1 h, and the pellet (p) and supernatant (s) fractions were analyzed by SDS–PAGE and quantitative Western blotting using antibodies against *T. gondii* actin and TgADF. Suppression of ADF was ~90% in this case, but more typically ranged from 97% to 98%. Quantitation of the actin bands (ACT) by phosphorimager analysis is depicted on the right. Bars represent means ± SD (n = 3 experiments where suppression ranged from 90% to 98%), ***$p \leq 0.001$. (B) Immunofluorescence analysis of actin in TgADF cKO parasites during gliding motility. TgADF cKO parasites were grown ± Atc for 66 h, harvested, and allowed to glide on coverslips before cells were fixed and stained with antibodies against *T. gondii* actin (shown in green) and the parasite surface antigen SAG (shown in red). Nuclei stained blue with DAPI. Suppression of TgADF resulted in cytoplasmic actin structures that were often concentrated at one or both poles of the parasite. Images were captured using wide-field microscopy and deconvolved using the nearest-neighbor algorithm. The micrographs represent a single slice taken from a z-stack. Scale bar: 2 μm. (C) Z-series of actin staining of a single TgADF cKO parasite from (B) treated with Atc, depicting the presence of actin structures in multiple planes of the parasite. Depth (in μm) of the depicted slice from the bottom of the parasite is given in the top right-hand corner. Scale bar: 2 μm.

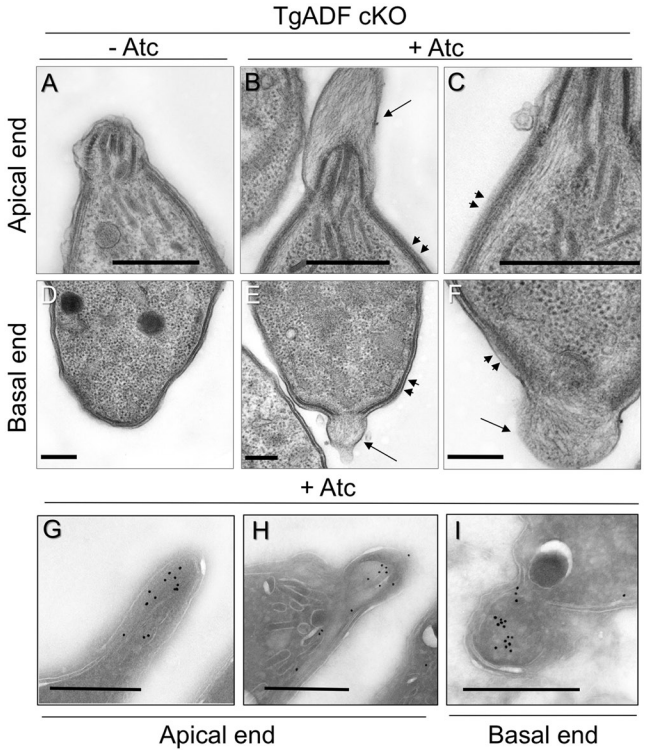

FIGURE 7: Ultrastructural analysis of actin filaments in *T. gondii* following TgADF suppression. Electron micrographs of extracellular TgADF cKO parasites after growth in the absence (–Atc) or presence of Atc (+Atc) for 66 h. The top panel depicts micrographs of the apical ends of parasites, whereas the bottom panel depicts the basal ends of different parasites. (A) Under normal conditions, actin filaments were not detected in parasites expressing TgADF. (B) When TgADF was suppressed, abundant actin filaments were detected in apical protrusions (single arrow) and just underneath the parasite plasma membrane (arrowheads). (C) Magnification of the region under the plasma membrane in a different parasite. (D) In TgADF cKO parasites grown in the absence of Atc, no filaments were detected at the basal ends, and the parasite plasma membrane and inner membrane were intact. (E) Suppression of TgADF resulted in actin filaments protruding from the basal end (arrow) accompanied by a gap in the inner membrane, and filaments were detected lining the inside of the plasma membrane (arrowheads). (F) Magnification of the posterior protrusion (arrow) and submembranous actin filaments (arrowheads) in a different parasite. (G–I) Cryoimmuno-EM localization of TgACT1 in the TgADF cKO cultured in Atc. Apical (G and H) and posterior (I) extensions were strongly stained for actin recognized by rabbit anti-TgACT1 antibody. Scale bar = 0.5 μm in all micrographs.

Actin-based motility is also a requirement for cell invasion by other apicomplexans, including *Plasmodium* (Miller *et al.*, 1979) and *Cryptosporidium* (Wetzel *et al.*, 2005). Plasmodium contains two ADF genes, and the orthologue of the one studied here, PfADF1, is essential in asexual stages, making direct analysis of its role in vivo difficult. In contrast, PfADF2, which more closely resembles ADF/cofilin proteins in higher eukaryotes, is not required during asexual stage development, and disruption of this gene shows a block in development of sporozoites, although it is not required for ookinete motility (Doi *et al.*, 2010).

T. gondii exhibits three stereotypical motility behaviors of which helical gliding is the only productive form of movement leading to host cell invasion (Håkansson *et al.*, 1999). Suppression of TgADF led to an almost complete loss of this productive movement and instead resulted in slow, serpentine movements, a pattern that has not been previously described for apicomplexan gliding motility. The absence of TgADF also led to reversals in direction of parasite movement, a behavior that does not occur in wild-type parasites (Håkansson *et al.*, 1999). Following TgADF suppression, some parasites started to move forward in one direction, but when they reached the point where only their posterior end was in contact with the substrate and their anterior end was raised, the parasite slid backward, sometimes repeating this motion a second time in the other direction. Suppression of TgADF also led to erratic rocking motions and uncoordinated behaviors.

Several behaviors observed in the absence of TgADF mimicked the effects of treatment with the actin-stabilizing compound JAS, which is a natural toxin produced by marine sponges (Crews *et al.*, 1986). For example, the decrease in host cell invasion following TgADF suppression is similar to treatment with low levels (i.e., 0.05–0.1 μM) of JAS, which corresponds to the dose at which actin polymerization is induced in parasites (Wetzel *et al.*, 2003). Suppression of TgADF also mimics the JAS-induced formation of spiral, filament-like clusters of actin in the parasite observed in immunofluorescence, and the apical filamentous protrusions seen by EM, features that are not normally seen in wild-type cells (Wetzel *et al.*, 2003). Finally, the erratic rocking and uncoordinated motility observed in time-lapse video microscopy are similar to features previously reported for JAS-treated cells (Wetzel *et al.*, 2003). Together these data indicate that the motility and invasion defects observed with suppression of TgADF are due to the stabilization of actin filaments within the parasite. Previous studies have stressed the inherent instability of *T. gondii* actin as responsible for the preponderance of G-actin in resting parasites (Sahoo *et al.*, 2006). Our studies, however, reveal that, in the absence of TgADF, a stable pool of assembled actin filaments now exists in the parasite, supporting an important role for TgADF in mediating actin dynamics in vivo. Based on the in vitro properties that we described previously (Mehta and Sibley, 2010), there are two likely mechanisms whereby TgADF might affect *T. gondii* actin. The role of TgADF in actin monomer sequestration may normally restrict the pool of monomers that is available for polymerization. We have previously estimated that the concentration of actin in *T. gondii* is ~8–10 μM (Sahoo *et al.*, 2006); however, using a more accurate estimation of cell volume (Rodrigues *et al.*, 2002) gives an estimate of ~40 μM actin. By comparison, the concentration of TgADF in the cell is ~35 μM, as determined by quantitative Western blotting of cell lysates compared with purified recombinant TgADF (unpublished data). Based on the previous estimate that TgADF has an affinity for G actin of ~0.8 μM (Mehta and Sibley, 2010), it is likely that a large fraction of G-actin remains sequestered in the cytosol by binding to TgADF. When TgADF was suppressed by addition of Atc, the concentration of TgADF dropped to ~2 μM (assuming 95% shutdown) favoring polymerization. Somewhat surprisingly, stable F-actin filaments were observed in the parasite under these conditions, despite the intrinsic instability of *T gondii* actin in vitro (Sahoo *et al.*, 2006). This observation suggests that the ability of TgADF to sever filaments may also have an important role in disassembling filaments in vivo, assuring the rapid turnover of subunits for new polymerization. Although we cannot distinguish the relative roles of these processes at present, their effects are expected to be additive, in both cases leading to an increased pool of F-actin.

Polymerization of actin filaments is required for gliding motility and cell invasion by *T. gondii*; hence it is somewhat paradoxical that enhanced filament stability disrupts these processes. The observed increase in F-actin in the absence of TgADF might be expected to decrease parasite motility for several reasons. First, it is possible that increased stability of F-actin is associated with less abundant monomer pools necessary for new filament formation, especially if the severing role of TgADF is important in filament turnover. Alternatively, it is possible that more abundant filaments or longer filaments, which are not seen in wild-type parasites, prevent normal gliding due to increased rigidity of the cell. Consistent with this model, the serpentine pattern of parasites gliding in the absence of TgADF form elongated trails that lack the tight helical arc of normal gliding (Håkansson *et al.*, 1999). An overabundance of longer filaments may also cause steric hindrance between actin filaments that are engaged with cell surface adhesive proteins and the myosin motor embedded in the inner membrane (Sibley, 2004). Finally, it is possible that a more stable actin cytoskeleton affects substrate interactions that are required for productive motility. Consistent with this model, recent studies using transitional force microscopy to examine gliding of *Plasmodium* sporozoites have revealed that increased stability of the F-actin cytoskeleton, induced by JAS treatment, is associated with decreased adhesion strength and eventual disruption of motility (Munter *et al.*, 2009). Further defining these roles will require more precise in vivo methods for elucidating the role of TgADF during temporal and spatial events important for motility. The normal abundance of G-actin in apicomplexans combined with less stable actin filaments results in a system that is optimized for rapid and efficient actin polymerization and turnover. TgADF plays a critical role in maintaining actin dynamics as shown by the enhanced stabilization of F-actin and the subsequent disruption of motility that occurs following suppression. Despite having a small cast of characters to orchestrate actin dynamics, apicomplexan parasites have devised an exquisitely efficient system to achieve rapid motility.

MATERIALS AND METHODS

Parasite culture

T. gondii tachyzoites were propagated by growth in monolayers of human foreskin fibroblasts (HFFs) cultured in DMEM (Invitrogen, Carlsbad, CA) supplemented with 10% fetal bovine serum (FBS), 2 mM glutamine, 20 mM HEPES (pH 7.5), and gentamycin at 20 μg/ml. Tetracycline-free FBS (HyClone, Logan, UT) was used when culturing the merodiploid and TgADF cKO parasite strains. Chloramphenicol (20 μg/ml; Sigma-Aldrich, St. Louis, MO), phleomycin (5 μg/ml; Invitrogen, San Diego, CA), and Atc (1.5 μg/ml; Clontech, Palo Alto, CA) were added to the medium as indicated.

Antibodies

TgADF was detected using a rabbit polyclonal antibody that was commercially generated (Covance Research Products, Denver, PA) against recombinant full-length TgADF cloned with a C-terminal His6x tag in the pET22b+ vector (Novagen, Darmstadt, Germany). Protein expression was induced by the addition of 1 mM isopropyl

β-D-1-thiogalactopyranoside, and the soluble fraction of TgADF was purified from *Escherichia coli* BL21 cells as previously described (Mehta and Sibley, 2010). Rabbit polyclonal antibodies to recombinant TgACT, expressed as a natively folded protein in baculovirus (Sahoo *et al.*, 2006), were also produced commercially. Aldolase was detected using rabbit polyclonal antisera to TgALD1 (Starnes *et al.*, 2006). The surface antigen SAG1 was detected using the mouse monoclonal antibody (mAb) DG52.

Generation of the TgADF cKO

The TgADF cKO was constructed using the Tet-TA system (Meissner *et al.*, 2002). *TgADF* (GenBank accession number AAC47717) was PCR amplified to include a C-terminal HA9 tag (primer sequences given in Supplemental Table S1) and cloned into the tetracycline-regulated expression vector pTetO7Sag4 using the Mfe1 and Pac1 restriction sites, generating the plasmid pS4ADFHA. (Description of strains and plasmids is given in Supplemental Table S2.) To provide selection, the *cat* gene (conferring chloramphenicol resistance) driven by the *SAG1* promoter was cloned into the *Xba*1 site on the plasmid backbone. This construct was transfected into a parasite line expressing the Tet-TA (Meissner *et al.*, 2002), referred to here as the Tet-TA strain (Supplemental Table S2), and, after two rounds of drug selection, stable transformants were single-cell cloned by limiting dilution. The resulting merodiploid clones were assayed by immunofluorescence and Western blotting to confirm regulated expression of TgADF-HA, and three clones were chosen to continue the experiments.

To generate the *TgADF* knockout construct (pADFKO), the *ble* selectable marker conferring phleomycin resistance driven by the *SAG1* promoter was flanked by genomic DNA sequences from 2 kb upstream and 2 kb downstream of the *TgADF* start and stop codons, respectively (Supplemental Table S1). A tandem YFP cassette driven by the α-tubulin promoter was placed downstream of the knockout cassette to provide a means for negative selection for double crossover events. pADFKO was linearized with the Apa1 restriction endonuclease and transfected into the chosen merodiploid clones. Phleomycin was used to select for stable transformants followed by fluorescence-activated cell sorting using a Dako MoFlo (Carpinteria, CA) to select for YFP-negative parasites that were cloned by limiting dilution. TgADF cKO clones were confirmed using diagnostic PCR primer pairs 1–2 and 3–4 (Supplemental Table S1).

Western blotting

Parasite lysates were resolved on 15% SDS–PAGE gels, transferred to membranes, and probed with rabbit anti-TgADF or rabbit anti-aldolase antibodies, followed by a peroxidase-conjugated goat anti–rabbit IgG (Jackson ImmunoResearch Laboratories, West Grove, PA). Chemiluminescence with ECL Plus (GE Healthcare, Piscataway, NJ) was used for detection, and bands were quantified using an FLA-5000 phosphorimager (Fuji Film Medical Systems, Stamford, CT).

Immunofluorescence microscopy

For detection of ADF protein shutdown by immunofluorescence microscopy, parasites were pretreated with Atc at 1.5 μg/ml for 24 h before infecting HFF monolayers grown on coverslips, followed by growth for an additional 24 h. Coverslips were fixed with 4% paraformaldehyde and permeabilized with 0.25% Triton X-100 before staining with anti-TgADF and anti-SAG primary antibodies followed by secondary antibodies conjugated to AlexaFluor 488 or AlexaFluor 594 (Invitrogen), respectively. Images were acquired using a Zeiss Axioskop 2 MOT Plus microscope equipped with a 63× 1.3 numerical aperture lens and an AxioCam Mrm camera (Carl Zeiss, Thornwood, NY). The same exposure time controlled by Axiovision v4.2 software was used for imaging different strains.

For detection of F-actin in parasites, freshly harvested parasites were resuspended in HHE buffer (Hanks Balanced Salts [Sigma], 1 mM EGTA, and 10 mM HEPES, pH 7.4), and parasites were allowed to glide on bovine serum albumin (BSA; 50 μg/ml)–coated coverslips for 15 min at 37°C, before cells were fixed with 4% paraformaldehyde and permeabilized with 0.25% Triton X-100. Parasites were stained with rabbit anti-TgACT and mouse anti-SAG1 antibodies, followed by AlexaFluor 488– and AlexaFluor 594–conjugated secondary antibodies, respectively. Samples were mounted in Pro-Long Gold anti-fade reagent containing 4′,6-diamidino-2-phenylindole (DAPI; Molecular Probes, Eugene, OR), and images were acquired as z-stack series (0.255-μm steps) using a Zeiss Axioskop 2 MOT Plus fluorescence microscope equipped with a 100×, 1.4 NA Plan Apochromat lens and an Axiocam Mrm monochrome camera (Carl Zeiss). Images were deconvolved in Axiovision version 4.5 software using the nearest-neighbor algorithm.

EM

Freshly harvested parasites were resuspended in HHE buffer, incubated for 15 min at 37°C, and fixed in 2% paraformaldehyde/2.5% glutaraldehyde (Polysciences, Warrington, PA) in 100 mM phosphate buffer, pH 7.2, for 1 h at room temperature. Samples were washed in phosphate buffer and postfixed in 1% osmium tetroxide (Polysciences) for 1 h. Following extensive washing in distilled water, samples were en bloc stained with 1% aqueous uranyl acetate (Ted Pella, Redding, CA) for 1 h. Samples were dehydrated in a graded series of ethanol and embedded in Eponate 12 resin (Ted Pella). Ultrathin sections were cut with a LeicaUltracut UCT ultramicrotome (Leica Microsystems, Bannockburn, IL) and stained with uranyl acetate and lead citrate. For cryoimmuno-EM, parasites were fixed in 4% paraformaldehyde/0.05% glutaraldehyde (Polysciences) in 100 mM PIPES buffer (pH 7.2). Samples were then embedded in 10% gelatin and infiltrated overnight with 2.3 M sucrose/20% polyvinyl pyrrolidone in PIPES at 4°C and frozen in liquid nitrogen. Ultrathin sections were cut with a cryo-ultramicrotome and probed with rabbit anti-TgACT antibody (1:600 [vol/vol]) (Dobrowolski *et al.*, 1997) followed by secondary anti-rabbit antibody conjugated to 18-nm colloidal gold and counterstaining with uranyl acetate/methylcellulose. Samples were viewed and photographed on a JEOL 1200 EX transmission electron microscope (JEOL USA, Peabody, MA), and images were adjusted linearly using Adobe Photoshop version 8.0.

Plaque assay

Plaque assays were performed as previously described (Roos *et al.*, 1994). Confluent monolayers of HFF cells grown in six-well plates were infected with 200 parasites per well, supplemented with Atc at 1.5 μg/ml as indicated. After 18 h of infection, extracellular parasites were removed and Atc was added back to the indicated wells at a concentration of 1 μg/ml. Monolayers were fixed with cold methanol 8 d after infection and were stained with 0.1% crystal violet. Experiments were repeated three times with triplicate wells per experiment.

Invasion assay

Two-color invasion assays were performed as previously described (Buguliskis *et al.*, 2010) with minor modifications. Freshly egressed parasites were resuspended in invasion medium (low bicarbonate DMEM, 20 mM HEPES, 3% FBS, pH 7.4) and added to subconfluent host cell monolayers seeded on coverslips. After a 1-min spin at

1000 rpm to deposit parasites onto the cell monolayer, invasion was allowed to proceed for 20 min at 37°C. Nonattached parasites were removed by washing with invasion medium, and cells were fixed with 2.5% paraformaldehyde for 15 min at 4°C. Extracellular parasites were detected with the DG52 mouse mAb to SAG1, directly conjugated to AlexaFluor 594. After permeabilization with 0.25% Triton X-100, all parasites were detected with the DG52 primary antibody, followed by the AlexaFluor 488 secondary antibody. Extracellular and intracellular parasites and host cell nuclei were counted from five fields per coverslip from three coverslips, in two independent experiments. Data are plotted as the average number of parasites per host cell as well as the percentage of total parasites invading host cells. Values represent the mean ± SD, n = 6.

Video microscopy

Time-lapse video microscopy was conducted using a Zeiss Axiovert phase-contrast microscope equipped with a temperature-controlled stage (Medical Systems, Greenvale, NY) to maintain 37°C incubation. Images were collected under low-light illumination using an intensified CCD C2400 camera (Hamamatsu Photonics K.K., Hamamatsu City, Japan) at 40× magnification, and images were acquired using OpenLab software (Improvision, Waltham, MA) to control the shutters and camera.

Ionophore-induced egress

HFF cells that had previously been seeded on glass-bottom culture dishes (MatTek, Ashland, MA) were infected with parasites that had been treated with Atc for one cycle, and were allowed to grow for an additional 24 h. Extracellular parasites were removed, and the medium was replaced with Ringer's solution containing 1% FBS. Dishes were allowed to equilibrate on a heated stage before the addition of 2 μM calcium ionophore A23187 (Calbiochem, EMD Chemicals, USA). Recording was started immediately, and egress was monitored for ~10 min with a 1-s delay between frames and exposure times of ~110 ms.

Quantitation of egress kinetics was based on the analysis of time-lapse videos. Approximately 30 vacuoles containing two to eight parasites per vacuole from two independent experiments were analyzed per strain. The time taken to initiate motility, egress of the first parasite from the vacuole, and complete egress of all the parasites from the vacuole, was recorded. In cases where not all the parasites left the vacuole, the time at which the last parasite egressed from the vacuole was recorded.

Analysis of gliding motility

Freshly egressed parasites were harvested and resuspended in Ringer's medium (155 mM NaCl, 3 mM KCl, 2 mM $CaCl_2$, 1 mM $MgCl_2$, 3 mM NaH_2PO_4, 10 mM HEPES, 10 mM glucose) and added to glass-bottom culture dishes that had previously been coated with BSA at 50 μg/ml and washed with phosphate-buffered saline. Parasites were allowed to settle for 2–3 min before recording was started. Time-lapse movies of at least 75 frames were collected, with exposure times ranging from 60 to 150 ms per frame and with a 1-s delay between frames.

For quantifying the type of motility, composite images were imported into ImageJ (http://rsb.info.nih.gov/ij/), the Cell Counter plug-in was used to count the total number of parasites, and the associated motility phenotype was scored by the observer, as described previously (Buguliskis *et al.*, 2010; Lourido *et al.*, 2010). Helical, circular, and twirling movements were defined as previously described (Hakansson, 1999). Nonmotile parasites were classified as parasites that were attached to the substratum but were either stationary or essentially remained in the same spot over the time period analyzed (but did not engage in twirling). New motility behaviors that were predominantly seen in the TgADF cKO + Atc included directional movement that resembled circular or helical patterns, but the parasite did not complete the full movement within the 75-frame time period analyzed; these were classified as short movements. Uncoordinated movement was defined as movement involving frequent reversals of direction and little net migration, and was observed as a side-to-side rocking behavior or a tumbling/rolling movement. Values for quantifying the type of motility were based on the quantification of six movies per condition, taken from two independent experiments. An average of 85 parasites were counted per video.

To calculate the speed of motility, parasites were chosen and tracked using the ImageJ particle tracker plug-in (https://weeman.inf.ethz.ch/ParticleTracker). Tracks were individually inspected for accuracy and were used to define the beginning and end of each trajectory. Speed was calculated by measuring a parasite's displacement and dividing by the time taken for that displacement. Values are based on the quantitation of at least 20 parasites per condition taken from at least three movies.

Actin sedimentation assay

Freshly harvested parasites were resuspended in actin stabilization buffer (25 mM HEPES, 10 mM EGTA, 2 mM $MgCl_2$, 125 mM KCl) and incubated at 37°C for 30 min. Reactions were supplemented with a final concentration of 1% Triton X-100, DNAse1 (10 μg/ml), protease inhibitor cocktail (E64 at 1 μg/ml; AEBSF at 10 μg/ml; TLCK at 10 μg/ml; leupeptin at 1 μg/ml), and 10% glycerol, and parasites were lysed for 1 h at room temperature. Membrane ghosts were removed by low-speed centrifugation at 1000 × *g* for 2 min, and supernatants were centrifuged at 350,000 × *g* for 1 h at 4°C (TL100 rotor, Beckman Optima TL Ultracentrifuge; Beckman Coulter, Fullerton, CA). Pellet samples were washed once with actin stabilization buffer, proteins were precipitated from the soluble fraction with acetone, and equal fractions of pellet and supernatant were resolved by 15% SDS–PAGE. Actin was detected by Western blot analysis with a rabbit anti-*T. gondii* actin antibody as described earlier in text.

Statistics

All results are presented as mean values ± SD or SEM. Unpaired, equal variance, two-tailed Student's *t* tests were used to determine the statistical significance of differences observed between indicated groups for parametric comparisons. The Mann–Whitney U test was used for nonparametric comparisons.

ACKNOWLEDGMENTS

We thank Wandy Beatty, Microbiology Imaging Facility, Washington University, for performing the EM; Keliang Tang and Jennifer Barks for expert technical assistance; Joel Shuman for developing the protocols for data analysis of video microscopy; and John Cooper and David Sept for helpful advice. This work was supported by a Washington University Morse/Berg Fellowship to S.M. and a National Institutes of Health Grant (AI 073155) to L.D.S.

REFERENCES

Bamburg JR (1999). Proteins of the ADF/cofilin family: essential regulators of actin dynamics. Annu Rev Cell Dev Biol 15, 185–230.

Baum J, Papenfuss AT, Baum B, Speed TP, Cowman AF (2006). Regulation of apicomplexan actin-based motility. Nat Rev Microbiol 4, 621–628.

Baum J, Tonkin CJ, Paul AS, Rug M, Smith BJ, Gould SB, Richard D, Pollard TD, Cowman AF (2008). A malaria parasite formin regulates actin polymerization and localizes to the parasite-erythrocyte moving junction during invasion. Cell Host Microbe 3, 188–198.

Bernstein BW, Bamburg JR (2010). ADF/cofilin: a functional node in cell biology. Trends Cell Biol 20, 187–195.
Buguliskis JS, Brossier F, Shuman J, Sibley LD (2010). Rhomboid 4 (ROM4) affects the processing of surface adhesins and facilitates host cell invasion by *Toxoplasma gondii*. PLoS Pathog 6, e1000858.
Carlier MF, Laurent V, Santolini J, Melki R, Didry D, Xia GW, Hong Y, Chua NH, Pantaloni D (1997). Actin depolymerizing factor (ADF/cofilin) enhances the rate of filament turnover: implication in actin-based motility. J Cell Biol 136, 1307–1323.
Crews P, Manes LV, Boehler M (1986). Jasplakinolide, a cyclodepsipeptide from the marine sponge, *Jaspis* spp. Tetrahedron Lett 27, 2797–2800.
Daher W, Plattner F, Carlier MF, Soldati-Favre D (2010). Concerted action of two formins in gliding motility and host cell invasion by *Toxoplasma gondii*. PLoS Pathog 6.
Dobrowolski JM, Niesman IR, Sibley LD (1997). Actin in the parasite *Toxoplasma gondii* is encoded by a single copy gene, *ACT1* and exists primarily in a globular form. Cell Motil Cytoskel 37, 253–262.
Dobrowolski JM, Sibley LD (1996). Toxoplasma invasion of mammalian cells is powered by the actin cytoskeleton of the parasite. Cell 84, 933–939.
Doi Y, Shinzawa N, Fukumoto S, Okano H, Kanuka H (2010). ADF2 is required for transformation of the ookinete and sporozoite in malaria parasite development. Biochem Biophys Res Commun 397, 668–672.
Endo T, Sethi KK, Piekarski G (1982). *Toxoplasma gondii:* calcium ionophore A23187-mediated exit of trophozoites from infected murine macrophages. Exp Parasitol 53, 179–188.
Håkansson S, Morisaki H, Heuser JE, Sibley LD (1999). Time-lapse video microscopy of gliding motility in *Toxoplasma gondii* reveals a novel, biphasic mechanism of cell locomotion. Mol Biol Cell 10, 3539–3547.
Lourido S, Shuman J, Zhang C, Shokat KM, Hui R, Sibley LD (2010). Calcium-dependent protein kinase 1 is an essential regulator of exocytosis in Toxoplasma. Nature 465, 359–362.
McGough A, Pope B, Chiu W, Weeds A (1997). Cofilin changes the twist of F-actin: implications for actin filament dynamics and cellular function. J Cell Biol 138, 771–781.
Mehta S, Sibley LD (2010). *Toxoplasma gondii* actin depolymerizing factor acts primarily to sequester G-actin. J Biol Chem 285, 6835–6847.
Meissner M, Schluter D, Soldati D (2002). Role of *Toxoplasma gondii* myosin A in powering parasite gliding and host cell invasion. Science 298, 837–840.
Messina M, Niesman IR, Mercier C, Sibley LD (1995). Stable DNA transformation of *Toxoplasma gondii* using phleomycin selection. Gene 165, 213–217.
Miller LH, Aikawa M, Johnson JG, Shiroishi T (1979). Interaction between cytochalasin B-treated malarial parasites and erythrocytes. J Exp Med 149, 172–184.
Munter S, Sabass B, Selhuber-Unkel C, Kudryashev M, Hegge S, Engel U, Spatz JP, Matuschewski K, Schwarz US, Frischknecht F (2009). Plasmodium sporozoite motility is modulated by the turnover of discrete adhesion sites. Cell Host Microbe 6, 551–562.
Ono S (2007). Mechanism of depolymerization and severing of actin filaments and its significance in cytoskeletal dynamics. Int Rev Cytol 258, 1–82.
Pinder JC, Fowler RE, Dluzewski AR, Bannister LH, Lavin FM, Mitchell GH, Wilson RJM, Gratzer WB (1998). Actomyosin motor in the merozoite of the malaria parasite, *Plasmodium falciparum*, implications for red cell invasion. J Cell Sci 111, 1831–1839.
Plattner F, Yarovinsky F, Romero S, Didry D, Carlier MF, Sher A, Soldati-Favre D (2008). *Toxoplasma* profilin is essential for host cell invasion and TLR11-dependent induction of an interleukin-12 response. Cell Host Microbe 3, 77–87.
Poupel O, Tardieux I (1999). *Toxoplasma gondii* motility and host cell invasiveness are drastically impaired by jasplakinolide, a cyclic peptide stabilizing F-actin. Microb Infect 1, 653–662.
Rodrigues CO, Ruiz FA, Rohloff P, Scott DA, Moreno SNJ (2002). Characterization of isolated acidocalcisomes from *Toxoplasma gondii* tachyzoites reveals a novel pool of hydrolyzable polyphosphate. J Biol Chem 277, 48650–48656.
Roos DS, Donald RGK, Morrissette NS, Moulton AL (1994). Molecular tools for genetic dissection of the protozoan parasite *Toxoplasma gondii*. Methods Cell Biol 45, 28–61.
Sahoo N, Beatty WL, Heuser JE, Sept D, Sibley LD (2006). Unusual kinetic and structural properties control rapid assembly and turnover of actin in the parasite *Toxoplasma gondii*. Mol Biol Cell 17, 895–906.
Schachtele C, Seifert R, Osswald H (1988). Stimulus-dependent inhibition of platelet aggregation by the protein kinase C inhibitors polymyxin B, H-7 and staurosporine. Biochem Biophys Res Commun 151, 542–547.
Schmitz S, Grainger M, Howell SA, Calder LJ, Gaeb M, Pinder JC, Holder AA, Veigel C (2005). Malaria parasite actin filaments are very short. J Mol Biol 349, 113–125.
Schüler H, Matuschewski K (2006). Regulation of apicomplexan microfilament dynamics by minimal set of actin-binding proteins. Traffic 7, 1433–1439.
Schuler H, Mueller AK, Matuschewski K (2005). A Plasmodium actin-depolymerizing factor that binds exclusively to actin monomers. Mol Biol Cell 16, 4013–4023.
Shaw MK, Tilney LG (1999). Induction of an acrosomal process in *Toxoplasma gondii*: visualization of actin filaments in a protozoan parasite. Proc Natl Acad Sci USA 96, 9095–9099.
Sibley LD (2004). Invasion strategies of intracellular parasites. Science 304, 248–253.
Starnes GL, Jewett TJ, Carruthers VB, Sibley LD (2006). Two separate, conserved acidic amino acid domains within the *Toxoplasma gondii* MIC2 cytoplasmic tail are required for parasite survival. J Biol Chem 281, 30745–30754.
Wetzel DM, Chen LA, Ruiz FA, Moreno SNJ, Sibley LD (2004). Calcium-mediated protein secretion potentiates motility by *Toxoplasma gondii*. J Cell Sci 117, 5739–5748.
Wetzel DM, Håkansson S, Hu K, Roos DS, Sibley LD (2003). Actin filament polymerization regulates gliding motility by apicomplexan parasites. Mol Biol Cell 14, 396–406.
Wetzel DM, Schmidt J, Kuhlenschmidt M, Dubey JP, Sibley LD (2005). Gliding motility leads to active cellular invasion by *Cryptosporidium parvum* sporozoites. Infect Immun 73, 5379–5387.
Yamashiro S, Mohri K, Ono S (2005). The two *Caenorhabditis elegans* actin-depolymerizing factor/cofilin proteins differently enhance actin filament severing and depolymerization. Biochemistry 44, 14238–14247.